J Mater Sci (2009) 44:441–448
DOI 10.1007/s10853-008-3121-0

Effect of reverse and cyclic shear on the work-hardening of AISI 430 stainless steel

Wellington Lopes · Elaine Carballo Siqueira Corrêa · Haroldo Béria Campos · Maria Teresa Paulino Aguilar · Paulo Roberto Cetlin

Received: 12 September 2008 / Accepted: 17 November 2008 / Published online: 11 December 2008

Abstract Sheet metal forming commonly involves various processing steps leading to complex strain paths. The work hardening of the metal under these circumstances is different from that observed for monotonic straining. The effect of the strain path on the hardening of materials is usually studied through sequences of standard mechanical tests, and the shear test is especially well adapted to such studies in sheet forming. Shear straining covering Bauschinger and cyclic strain paths were used in the analysis of the hardening of AISI 430 stainless steel sheets. The tests were conducted at 0°RD, 45°RD, and 90°RD (Rolling Direction) and for three effective strain amplitudes. The results indicate that the material presents Bauschinger effects and strain hardening transients that are sensitive to the testing direction. In addition, the cyclic straining leads to an oscillating stress pattern for the forward and reverse shearing cycles, which depends on the deformation amplitude.

W. Lopes · P. R. Cetlin (✉)
Department of Metallurgical and Materials Engineering, Federal University of Minas Gerais, Rua Espírito Santo 35, s214, Centro, 30160-030 Belo Horizonte, Minas Gerais, Brazil
e-mail: pcetlin@demet.ufmg.br

E. C. S. Corrêa
Federal Center of Technological Education of Minas Gerais, CEFET/MG, Av. Amazonas 5253, Nova Suiça, 30480-000 Belo Horizonte, Minas Gerais, Brazil

H. B. Campos
Department of Mechanical Engineering, Federal University of Minas Gerais, Av. Antônio Carlos 6627, Pampulha, 32270-901 Belo Horizonte, Minas Gerais, Brazil

M. T. P. Aguilar
Department of Materials and Construction Engineering, Federal University of Minas Gerais, Rua Espírito Santo 35, Centro, 30160-030 Belo Horizonte, Minas Gerais, Brazil

Introduction

Sheet metal forming comprises a series of plastic straining operations, such as deep drawing and stretching providing the desired shape to the metal (in this case, to the sheet blank) through the use of dies and punches. In addition to the significant versatility in terms of the shapes obtained, numerous advantages are associated with these operations, such as high productivity, relatively low energy consumption, and reduced processing time. Therefore, a pronounced demand for sheet forming products has been observed, especially in the automotive, the aeronautic, and the appliance industries [1].

Many investigations have been conducted in order to improve sheet metal forming, involving various aspects such as the tooling features [2] and the effects of the process parameters on the materials formability. In this case, numerical techniques, especially the finite element method (FEM), have been widely employed [3, 4]. On the other hand, the classical approaches to the forming processes are based on the evaluation of simulative tests, such as the forming dome limit LDH [5], the Swift cup, the Erichsen Olsen dome [6], and the Nakazima tests [7]. Regarding specifically the automotive industry, the forming limit diagram (FLD) [8] and the forming limit stress diagram (FLSD) [9] are frequently employed in these studies.

Detailed information concerning both the strain history and the work hardening evolution of the metal under processing is necessary in the previously mentioned analyses, preferably involving conditions similar to those observed

in industrial operations and, therefore, including the prevailing complex deformation and/or stress states and paths. Nevertheless, the work hardening behavior of materials is usually taken as the one described by flow curves obtained through standard mechanical tests, i.e., monotonic straining processes (tension, compression, etc.). Hence, the results from these experiments usually do not reflect the exact non-monotonic deformation conditions developed in some industrial processes [10].

A reduction in the flow stress of the material, as well as work hardening transients, is commonly observed after strain path changes. The occurrence of reloading yield stresses lower than the flow stress at the end of the pre-strain (Bauschinger Effect, BE) has been attributed to the reorientation of internal stresses caused by grain incompatibilities and to the rearrangement of dislocations [11]. When the loading path is reversed, the internal stresses act in the same direction as the applied stresses, causing lower flow stresses in comparison with the monotonic test. The magnitude of this effect depends, among other parameters, on the pre-strain value, on the materials structural characteristics [12, 13], and, especially, on the mode of deformation [14, 15] in which magnitude of the strain path change is usually indicated by the α parameter [16].

The hardening transients have been associated with various causes: structural aspects related to the evolution of the dislocation substructure and a subsequent strain localization due to the development of shear microbands [17], a prevailing high density of dislocations [18], the nature of the dislocations generated during the pre-strain and their rearrangement during reloading [19], and the crystallographic texture [20]. Regarding the substructural aspects, the transient would be connected to the partial dissolution of the dislocation substructure generated in the pre-strain. The intensity of the initial decrease in the hardening rate increases with the pre-strain value [12]. Wilson and Bate [21] concluded that the magnitude of the reloading yield stress and the amplitude of the ensuing hardening transient depend on the strength of the dislocation walls generated in the pre-strain, where the dislocations accumulate at barriers in tangles and eventually form cells. These are strong barriers to dislocation glide in the slip systems intersecting the walls. The effective strength of these walls would depend on the local dislocation density, the strain path mode, and the pre-strain value.

Straining sequences of shear loading tests are known to be an effective way to investigate the plastic behavior of metals under real forming circumstances [1]. Various sequences have been studied, such as tension-cyclic torsion, equibiaxial stretching-tension, fatigue-tension, and tension-compression [22–26]. In addition to these procedures, the more recent planar shear technique is an efficient alternative method for the study of the effects of the strain path on the forming of metal sheets [27, 28]. In contrast to the former testing techniques, the latter method does not require long time-consuming experiments and complex laboratory equipments. Moreover, it lends itself easily to reverse shear deformation (Bauschinger type experiments), as well as to the achievement of high plastic straining levels [29]. Finally, various strain path change experiments can be conducted through planar shear, leading to flow curves closer to those related to real forming operations.

The investigations utilizing strain path changes and the shear test have involved, in general, low carbon steel [1, 19, 27], aluminum alloys [30] and, recently, Dual Phase (DP) steel [13]. However, no tests have been reported on AISI 430 stainless steel.

The aim of the present investigation is to analyze the work hardening behavior of AISI 430 stainless steel sheets submitted to strain path changes through the planar shear technique, covering a simple reversion of straining (BE) and cyclic testing.

Material and methods

The material used in this research was a AISI 430 stainless steel (sheets) with the following chemical composition (weight percent): 0.02C, 0.20Mn, 16.11Cr, 0.17Ni, 0.40Nb, and 0.01Ti. The specimens, used in their as-received state, were 0.60-mm thick, 50-mm long, and 15-mm wide. The shear zone gauge width was 3.50 mm.

The test apparatus consisted of an Instron model 5582 machine specially adapted for shear testing, based on the investigations developed by Rauch [27]. The shear strain rate was 0.002 s^{-1}.

(1) *Bauschinger*: forward shear test up to a shear strain γ of 0.30 followed by shear in the opposite (reverse) sense. The specimens submitted to Bauschinger tests were sheared at 0°, 45°, and 90° from the rolling direction (RD);
(2) *Cyclic shear sequences* (reverse, forward, and reverse straining) conducted with shear strain amplitudes of 0.22, 0.37, and 0.56, preceded by a shear pre-strain whose values were 0.11, 0.18, and 0.28, respectively. In this case, all samples were cut at 90° to the rolling direction (RD).

Figure 1a, b displays schematically the experimental straining sequences for the Bauschinger and cyclic sequences, respectively, in terms of the shear stress–shear strain curves and of the specimen employed in this test.

Monotonic shear tests were also performed, allowing a comparison with the results from the Bauschinger/cyclic shear tests. All shear stress–shear strain data were

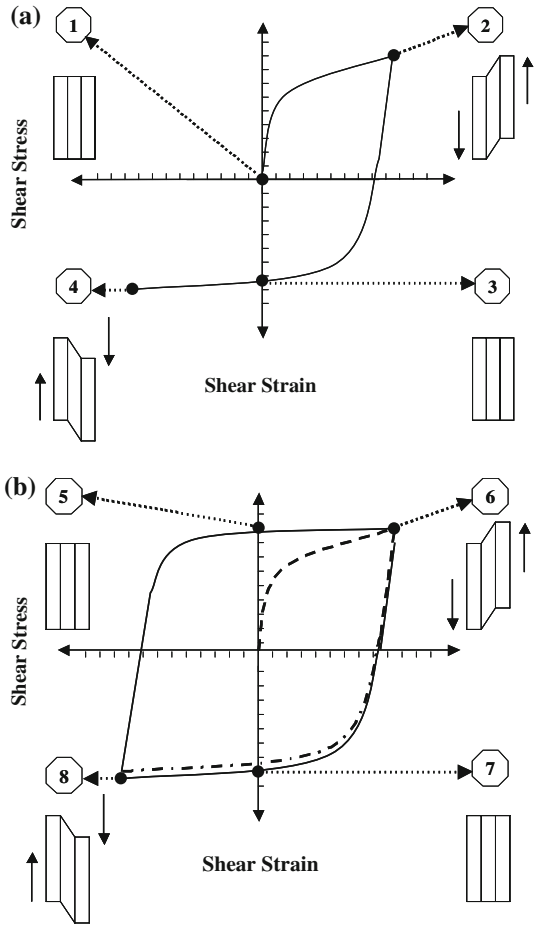

Fig. 1 Schematic cyclic shear experiment: **a** shear pre-strain and first reverse shear and **b** forward and second reverse shear

converted into effective stress–effective strain curves using the conversion parameter cited by Rauch [27]:

$$\sigma_e = 1.84\tau \quad (1)$$

$$\varepsilon_e = \lambda/1.84 \quad (2)$$

where σ_e is the effective stress, ε_e is the effective strain, τ is the shear stress, and γ is the shear strain.

In order to avoid the overlapping of the results and to clarify the analysis, the effective stress–effective strain curves were plotted according to the sequence shown in Fig. 2, for one complete deformation cycle, and where the reverse shearing is represented with a dashed line. The shear stress–shear strain results obtained in the experiments are exhibited in Fig. 2a. The shear deformation was converted into effective deformation employing Eq. 2 and thus taken only as positive and accumulative, i.e., the increments of deformation were added, as shown in Fig. 2b. The effective stresses were calculated using expression 1 and considered always positive, as shown in Fig. 2c. All cyclic experiments began with a shear pre-strain whose value was one-half of the total shear strain amplitude employed in the tests.

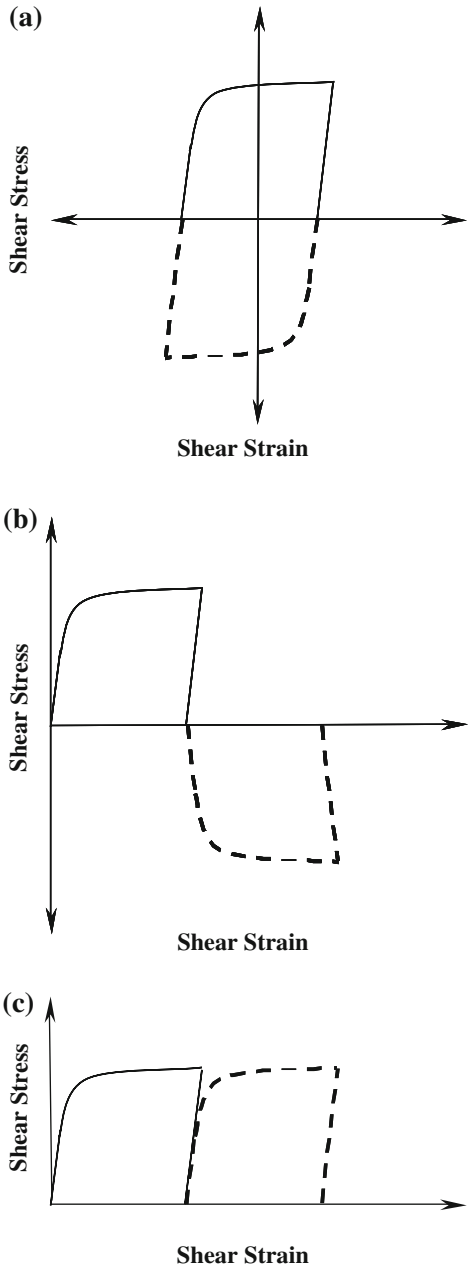

Fig. 2 Procedure employed to prepare the effective stress–effective strain curves related to the reverse and the cyclic tests

Results and discussion

Bauschinger shear test

Figure 3 shows the effective stress–effective strain curves of the AISI 430 stainless steel samples (sheared at 0°, 45°, and 90° to the rolling direction) submitted to a reverse shear sequence. In addition to the second stage flow curves, the monotonic shear test results are also displayed, in order to compare the mechanical behaviors with and without the

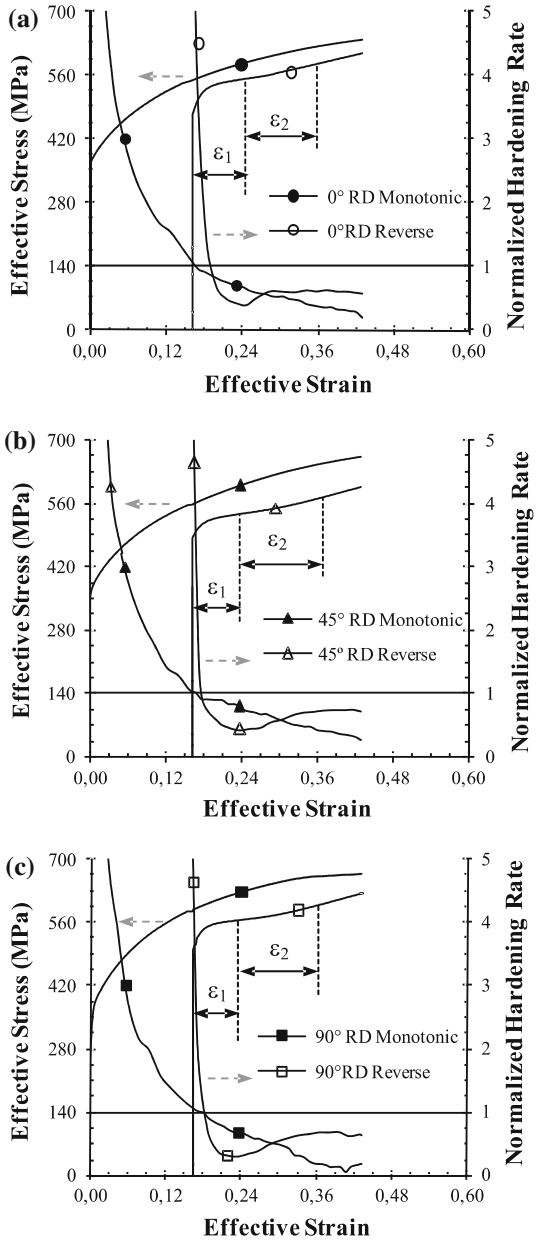

Fig. 3 Effective stress–effective strain and hardening rate–effective strain curves of the AISI 430 stainless steel subjected to pure and Bauschinger shear experiments: **a** 0°RD, **b** 45°RD, and **c** 90°RD

strain path change. The effective stress–effective strain data for both situations allowed the calculation of normalized hardening rates, i.e., the hardening rate (θ) multiplied by the inverse of the stress ($1/\sigma$), whose relationship with the strain is also exhibited in Fig. 3 (right vertical axis) [30].

For all the investigated conditions, the reverse shear flow curves display lower stress values than those observed in the monotonic shear experiment, i.e., the occurrence of the Bauschinger Effect is noted. The effect is more pronounced in the 90°RD samples, where the differences ($\Delta\sigma$) between the reloading stresses and the stresses in the monotonic test (at the same strain level) are about 90 MPa. For 45°RD and 0°RD, $\Delta\sigma$ values are $\sim$87 and $\sim$76 MPa, respectively.

At the beginning of all the reverse tests the normalized hardening rate $\theta(1/\sigma)$ falls abruptly to values below those observed for monotonic shear (at the same level of strains), increases to above the monotonic behavior and then stabilizes. In Fig. 3, ε_1 and ε_2 represent the deformation ranges associated with this unusual behavior. ε_1 corresponds to the region of the $\theta(1/\sigma)$ vs. ε curve where the hardening rate decreases with the deformation, whereas ε_2 is related to the opposite situation. In a similar manner as does $\Delta\sigma$, both ε_1 and ε_2 depend on the angle of the testing of the samples in relation to the rolling direction.

The rapidly falling values of $\theta(1/\sigma)$ indicate an intense occurrence of dynamic recovery processes during the strain interval ε_1 [31]. On the other hand, further straining with the magnitude ε_2 not only stabilizes the falling hardening, but actually involves an increase in $\theta(1/\sigma)$ at levels above those for monotonic straining (at the same levels of strain). The difference between ε_2 and ε_1 has been used by Vincze et al. [19] as an indication of the susceptibility of the material to hardening transients after changes in strain paths. Low values of ε_1 are associated with initially high work hardening instability, whereas high values of ε_2 are associated with the slow rates of hardening increase after the initial instability. Thus, samples displaying high values of $\varepsilon_2 - \varepsilon_1$ are the ones initially more sensitive to strain path changes and then the slowest to reach a final stable hardening rate. The lowest value of $\varepsilon_2 - \varepsilon_1$ was obtained for 0°RD, (0.111), whereas 45°RD and 90°RD presented the values of 0.128 and 0.132, respectively.

The above phenomena have been associated with the various causes presented before and especially with the substructural evolution of the material during the strain path change [18].

Cyclic shear sequence

Figure 4 shows the shear stress–shear strain responses of the AISI 430 stainless steel at 90°RD observed during the cyclic straining experiments (total shear strain amplitude $\Delta\gamma$ of 0.22, 0.37, and 0.56, corresponding to total effective strain amplitudes $\Delta\varepsilon$ of 0.12, 0.20, and 0.30, respectively). The cyclic tests were conducted only at 90°RD because this direction presented the longest hardening transient ($\varepsilon_2 - \varepsilon_1 = 0.132$) in the strain reversal tests, and would thus probably show more pronounced strain path effects under cyclic straining.

In order to allow a more detailed evaluation of the mechanical behavior of the metal, the effective stress–effective strain curves during the cyclic loading (determined from the results in Fig. 4) and the normalized

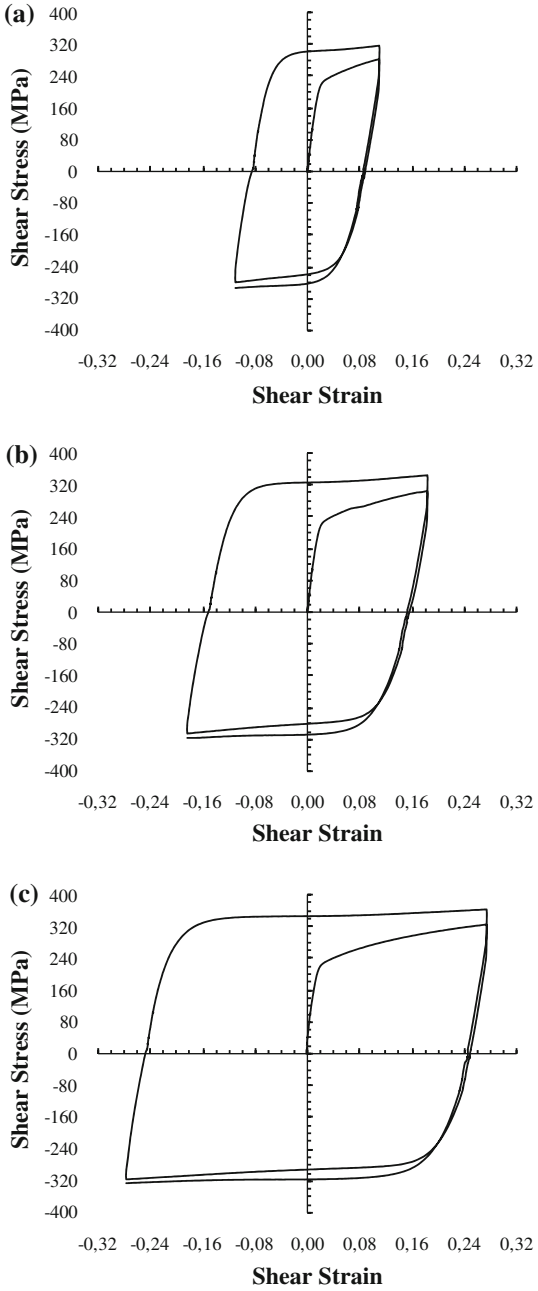

Fig. 4 Shear stress–shear strain curves of the AISI 430 stainless steel samples at 90°RD obtained in cyclic experiments—shear strain amplitude: **a** 0.22, **b** 0.37, and **c** 0.55

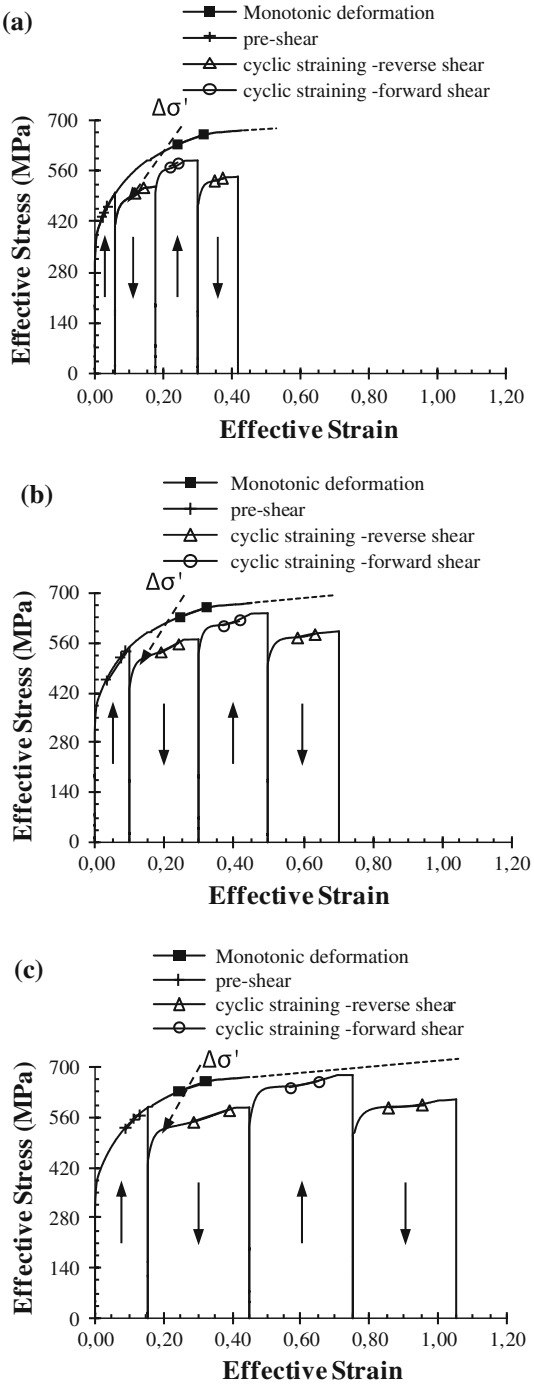

Fig. 5 Effective stress–effective strain curves of the AISI 430 stainless steel samples at 90°RD subjected to monotonic and cyclic shear experiments—effective strain amplitude: **a** 0.12, **b** 0.20, and **c** 0.30

hardening rate–effective strain curves are exhibited on Figs. 5 and 6, respectively. These graphs were plotted in the similar manner as shown in Fig. 3, i.e., all values of stress were considered positive and the deformation was accumulative. The arrows shown in the graphs correspond to the directions of shear straining (↑ forward and ↓ reverse).

Figure 5 indicates that the cyclic shearing led to less hardening than monotonic straining for the AISI 430 steel, and Fig. 4 suggests a hardening saturation at the end of the processing (after the second reverse shear), for all the strain amplitudes. This saturation stress increases with $\Delta\gamma$, as shown in Table 1. There is a clear, but slow hardening caused by the increasing straining.

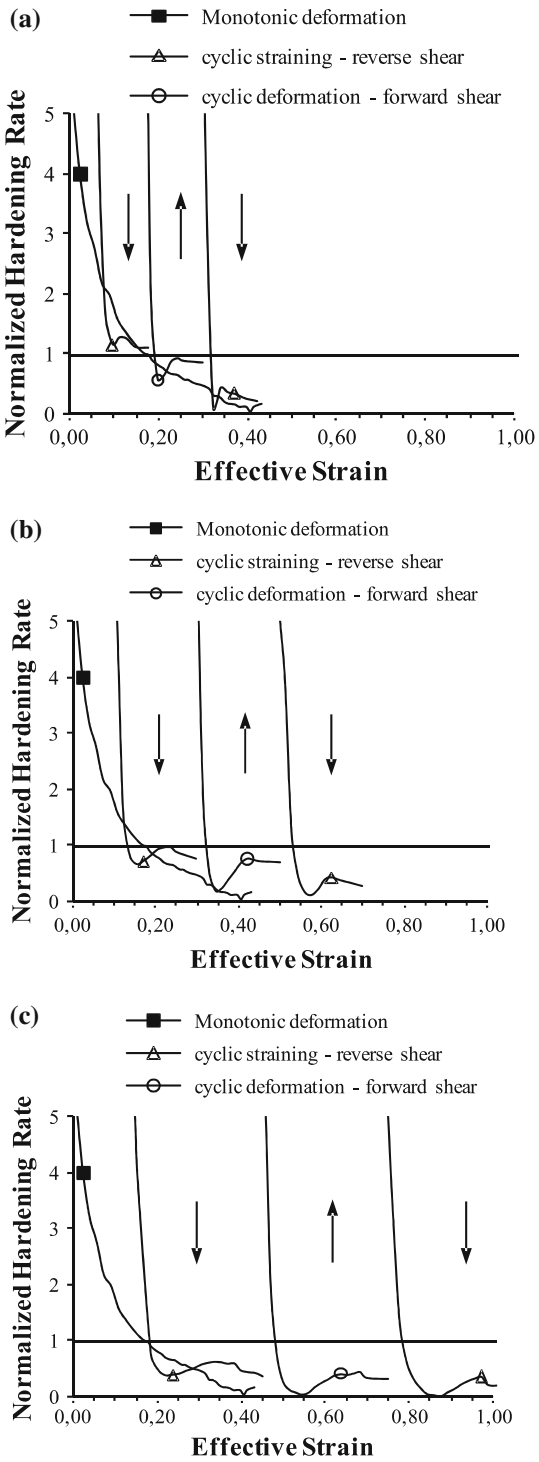

Fig. 6 Normalized hardening rate–effective strain curves of the AISI 430 stainless steel samples at 90°RD subjected to monotonic and cyclic shear experiments—effective strain amplitude: **a** 12%, **b** 20%, and **c** 30%

Considering the two first deformation steps in Fig. 5 (a forward and a reverse deformation), the differences in stress between the yield stress in the first reverse deformation and the stress at the end of the first forward cycle under monotonic shearing ($\Delta\sigma'$) were found to be 87, 123, and 156 MPa, corresponding to the effective strain amplitudes $\Delta\varepsilon$ of 0.12, 0.20, and 0.30, respectively. As previously stated, the higher values of $\Delta\sigma'$ associated with the increasing straining amplitudes $\Delta\varepsilon$ are a typical result of the BE [12, 30, 31].

On the other hand, the values of $\Delta\sigma'$ for the next forward deformation steps are clearly lower than those for the previous step, and their magnitudes decrease with an increase in strain amplitude. These results are the opposite of those observed in the previous deformation step. This is probably associated with the fact that the first reverse deformation did not completely replace the dislocation structure and stress fields originated in the first forward step with structures and stress fields typical of only the reverse deformation. This is demonstrated by the comparison of the yield strength of the material in the 2nd forward cycle, (σ_{y2}) and the stress at the end of the 1st reverse cycle (σ_{f1}) shown in Table 2. For a low strain amplitude (Fig. 5a), $\sigma_{y2} > \sigma_{f1}$ because the low strain amplitude had a limited effect on the disruption of the stress fields caused by the previous deformation step. As the deformation amplitude in the 1st reverse step increases, more and more disruption of these previous dislocation structures and stress fields occur, and σ_{y2} becomes increasingly lower than (σ_{f1}), as displayed in Fig. 5b, c.

The stresses in the 2nd reverse cycle are lower than in the previous forward cycle, exactly like the situation after the 1st forward cycle. The cause for this situation is similar to that previously discussed and associated with the degree of disruption in the internal stress fields of the material caused by the sequence of previous cycles. As the number of cycles increases, a steady state will eventually be reached, as has been amply demonstrated for the warm and hot cyclic torsion of copper and IF steel [32, 33] and by the

Table 1 Saturation shear stresses for AISI 430 under cyclic tests

Shear strain amplitude	Saturation shear stress (MPa)
0.22	290
0.37	314
0.55	324

Table 2 Comparison of the flow stress at the end of the 1st reverse cycle (σ_{f1}), and the yield strength in the 2nd forward cycle (σ_{y2}) for the various strain amplitudes

Effective strain amplitude	σ_{f1} (1st reverse cycle, MPa)	σ_{y2} (2nd forward cycle, MPa)	$\sigma_{y2} - \sigma_{f1}$ (MPa)
0.12	497	499	2
0.20	543	522	−21
0.30	585	527	−58

cyclic shear tests on the aluminum 3004 alloy in the recovered state [34].

The hardening rate–effective strain curves displayed in Fig. 6 also reveal the influence of the cyclic strain amplitude on the mechanical behavior of the metal. For all conditions evaluated in the investigation, analogously to the Bauschinger experiments, there is an initial sharp fall in the $(\theta)(1/\sigma)$ after all strain path changes, which is followed by an increasing $(\theta)(1/\sigma)$, which then stabilizes to a value higher than the corresponding one for monotonic shear.

Figure 6 indicates that the higher strain amplitudes are also associated with increasing strains during the transient (both ε_2 and ε_1), in a similar way as to the observations of Hu [29] for mild steel under cyclic deformation. For the 2nd second forward cycle, for example, as the strain amplitude increases not only are the $\Delta\sigma'$ values lower, but the longer transients also allow more work hardening of the material at the end of the cycle, resulting in a flow curve closer to the monotonic curve than in the case of the first reverse cycle. It is again believed that longer hardening transients, which are associated with the higher strain amplitudes, are caused by the higher level of disruption of the substructure caused by the previous deformation step. According to this reasoning, small successive deformation steps will cause little work hardening of the material, whereas large steps will approximately reproduce the monotonic curve, probably at a lower level caused by the BE. This has been confirmed for the warm and hot cyclic torsion of IF steels and copper [32, 33].

Conclusions

The strain path changes under Bauschinger and cyclic shear tests in AISI 430 stainless steel sheets indicated that

(1) Increasing levels of the superimposed reversed shearing initially lead to increasingly lower work hardening, in relation to the hardening caused by tension. However, above a certain reversed shearing level, the work hardening ceases to decrease and then increases.
(2) The cyclic straining led to an oscillating stress pattern for successive deformation cycles, probably caused by the incomplete disruption of the dislocation structure and stress fields associated with the successive deformation steps.
(3) The deformation range, where work hardening transients caused by cyclic straining are observed, increases as the deformation amplitude is increased.

Acknowledgements The authors acknowledge the financial support for this research by CAPES (Coordenação de Aperfeiçoamento de Pessoal de Nível Superior) and CNPq (Conselho Nacional de Desenvolvimento Científico e Tecnológico).

References

1. Nesterova EV, Bacroix B, Teodosiu (2001) Mater Sci Eng A 309–310:495. doi:10.1016/S0921-5093(00)01639-7
2. Dejmal I, Tirosh J, Shirizly A, Rubinsky L (2002) Int J Mech Sci 44:1245. doi:10.1016/S0020-7403(02)00019-X
3. Kobayashi S, Oh SI, Altan T (1988) Metal forming and the finite-element method. Oxford University Press, New York, USA
4. Lim TC, Ramakrishna S, Shang HM (1999) J Mater Process Technol 30:495. doi:10.1016/S1359-8368(99)00015-3
5. Karthik V, Comstock RJ Jr, Hershberger DL, Wagoner RH (2002) J Mater Process Technol 121:350. doi:10.1016/S0924-0136(01)01219-5
6. Doyle LE, Morris JL, Leach JL, Schrader GF (1978) Processos de Fabricacão e Materiais para Engenheiros, 2nd edn. Edgard Blücher, São Paulo, Brazil
7. Nakazima K, Kikuma T, Hasuka K (1968) Yamata Tech Rep 264:141
8. Gosh AK, Hecker SS, Keeler SP (1984) In: Dieter GE (ed) Workability testing techniques. American Society for Metal, Metals Park, London, England
9. Arrieux R (1997) J Mater Process Technol 64:25. doi:10.1016/S0924-0136(96)02550-2
10. Kuroda M, Tvergaard V (2000) Int J Mech Sci 42:867. doi:10.1016/S0020-7403(99)00029-6
11. Barlat F, Ferreira Duarte JM, Gracio JJ, Lopes AB, Rauch EF (2003) Int J Plast 19:1215. doi:10.1016/S0749-6419(02)00020-7
12. Wilson DV, Zandrahimi M, Roberts WT (1990) Metall Mater 38:215. doi:10.1016/0956-7151(90)90051-H
13. Haddadi H, Bouvier S, Banu M, Maier C, Teodosiu C (2006) Int J Plast 22:2226. doi:10.1016/j.ijplas.2006.03.010
14. Côrrea ECS, Aguilar MTP, Cetlin PR (2000) J Mater Sci Lett 779:781. doi:10.1023/A:1006768706054
15. Mazilkin AA, Straumal BB, Protasova SG, Dobatkin SV, Baretzky B (2008) J Mater Sci 3800:3805. doi:10.1007/s.10853-007-2222-5
16. Schmitt JH, Aernoudt E, Baudelet B (1985) Mater Sci Eng A 75:13
17. Rauch EF, G'Sell C (1989) Mater Sci Eng A 111:71. doi:10.1016/0921-5093(89)90199-8
18. Rauch EF, Gracio JJ, Barlat F (2007) Acta Mater 55:2939. doi:10.1016/j.actamat.2007.01.003
19. Vincze G, Rauch EF, Gracio JJ, Barlat F, Lopes AB (2005) Acta Mater 53:1005. doi:10.1016/j.actamat.2004.10.046
20. Lopes AB, Rauch EF, Gracio JJ (1999) Acta Mater 47:859. doi:10.1016/S1359-6454(98)00417-0
21. Wilson DV, Bate PS (1994) Acta Metall Mater 42:1099. doi:10.1016/0956-7151(94)90127-9
22. Sillekens WH, Dautzenberg JH, Kals J (1991) Proc 'International Institution for Production Research—CIRP', vol 40, p 255
23. Corrêa ECS, Aguilar MTP, Silva EMP, Cetlin PR (2003) J Mater Process Technol 142:282. doi:10.1016/S0924-0136(03)00575-2
24. Jia WP, Fernandes JV (2003) Mater Sci Eng A 348:133. doi:10.1016/S0921-5093(02)00630-5
25. Boger RK, Wagoner RH, Barlat F, Lee MG, Chung K (2005) Int J Plast 21:2319. doi:10.1016/j.ijplas.2004.12.002
26. Chung JH, Lee DN (1993) J Mater Sci 4704:4712. doi:10.1007/BF00414261
27. Rauch EF (1992) Solid State Phenom 23:317
28. Bouvier S, Haddadi H, Levée P, Teodosiu C (2006) J Mater Process Technol 172:96. doi:10.1016/j.jmatprotec.2005.09.003
29. Hu Z (1994) Acta Metall Mater 42:3481. doi:10.1016/0956-7151(94)90480-4

30. Zandrahimi M, Platias S, Price D, Barrett D, Bate PS, Roberts WT, Wilson DV (1989) Metall Mater Trans A 20:2471
31. Boger RK (2006) Non-monotonic strain hardening and its constitutive representation. Ph.D. thesis, Ohio State University, Ohio
32. Pinheiro IP, Barbosa R, Cetlin PR (2006) ISIJ Int 46:734
33. Pinheiro IP, Barbosa R, Cetlin PR (2007) Mater Sci Eng A 458:136. doi:10.1016/j.msea.2006.12.046
34. Dirras GF, Duval JL, Swiatnicki W (1999) Mater Sci Eng A 263:85. doi:10.1016/S0921-5093(98)01082-X